This article was downloaded by:
On: *24 January 2011*
Access details: *Access Details: Free Access*
Publisher *Taylor & Francis*
Informa Ltd Registered in England and Wales Registered Number: 1072954 Registered office: Mortimer House, 37-41 Mortimer Street, London W1T 3JH, UK

Journal of Macromolecular Science, Part A
Publication details, including instructions for authors and subscription information:
http://www.informaworld.com/smpp/title~content=t713597274

NOVEL CERAMER MATERIALS BASED ON JEFFAMINE® POLY(PROPYLENE OXIDE) OLIGOMERS AND TETRAMETHOXYSILANE

Kurt Jordens[a]; Garth Wilkes[b]
[a] Texas Eastman Division, Eastman Chemical Company, Longview, TX, U.S.A. [b] Department of Chemical Engineering, Polymer Materials and Interfaces Laboratory, Virginia Polytechnic Institute and State University, Blacksburg, Virginia, U.S.A.

Online publication date: 14 February 2000

To cite this Article Jordens, Kurt and Wilkes, Garth(2000) 'NOVEL CERAMER MATERIALS BASED ON JEFFAMINE® POLY(PROPYLENE OXIDE) OLIGOMERS AND TETRAMETHOXYSILANE', Journal of Macromolecular Science, Part A, 37: 3, 145 — 175
To link to this Article: DOI: 10.1081/MA-100101086
URL: http://dx.doi.org/10.1081/MA-100101086

PLEASE SCROLL DOWN FOR ARTICLE

Full terms and conditions of use: http://www.informaworld.com/terms-and-conditions-of-access.pdf

This article may be used for research, teaching and private study purposes. Any substantial or systematic reproduction, re-distribution, re-selling, loan or sub-licensing, systematic supply or distribution in any form to anyone is expressly forbidden.

The publisher does not give any warranty express or implied or make any representation that the contents will be complete or accurate or up to date. The accuracy of any instructions, formulae and drug doses should be independently verified with primary sources. The publisher shall not be liable for any loss, actions, claims, proceedings, demand or costs or damages whatsoever or howsoever caused arising directly or indirectly in connection with or arising out of the use of this material.

J.M.S.—PURE APPL. CHEM., A37(3), pp. 145–175 (2000)

NOVEL CERAMER MATERIALS BASED ON JEFFAMINE® POLY(PROPYLENE OXIDE) OLIGOMERS AND TETRAMETHOXYSILANE

Kurt Jordens† and Garth Wilkes*

Department of Chemical Engineering
Polymer Materials and Interfaces Laboratory
Virginia Polytechnic Institute and State University
Blacksburg, Virginia 24061-0211

Downloaded At: 12:47 24 January 2011

Key Words: Ceramer, Inorganic–Organic Hybrid, Sol-Gel, Nanocomposite, Poly(Propylene Oxide), Tetramethoxysilane

ABSTRACT

Novel hybrid organic–inorganic network materials have been generated based on poly(propylene oxide) (PPO) and tetramethoxysilane (TMOS). The PPO source chosen for this study was the family of JEFFAMINE®s often employed as epoxy curing agents. These materials were end–functionalized with trialkoxysilane groups which later were exploited in the sol–gel reaction. The sol–gel variables of water and acid catalyst concentration had little influence on the final structure and properties of the resulting network materials for the ranges probed. Increasing the TMOS content, however, generated a structure that angle X-ray scattering revealed a correlation length associated with a silicate phase separated by PPO chains, which increased with PPO molecular weight, as expected.

* Author to whom correspondence should be addressed.

† Present address: Texas Eastman Division, Eastman Chemical Company, P.O. Box 7444, Longview, TX 76507-7444.

Copyright © 2000 by Marcel Dekker, Inc. www.dekker.com

INTRODUCTION

Due to the versatile nature of the sol–gel reaction, many novel and interesting materials have been generated by this process [1]. One advantage of the technique is that very high purity reactants can be employed since the metal alkoxide monomers are usually liquids, and can be distilled to high purity. It is also relatively simple to incorporate organic materials into network oxides through the sol–gel reaction under the proper conditions. There are three known ways to generate hybrid inorganic–organic materials by the sol–gel route [2]; firstly, due to the porous nature of the oxide gels created from the sol-gel approach, organic materials can be impregnated into the voids thereby forming the hybrid. There are no covalent bonds between the organic and inorganic components by this route. An example of this type of hybrid was prepared by Pope and Mackenzie [3] and Abramoff and Klein [4] involving the impregnation of the pores of silica gel with liquid methylmethacrylate which is subsequently polymerized to yield a transparent hybrid film. In the second route, the organic material can be added to the sol-gel reaction before gelation when the mixture is still in a liquid state. Formation of the inorganic network oxide then traps the organic component within the crosslinked inorganic structure. Hybrids prepared in this way also do not possess covalent links between the two components. Oxide gels have been impregnated by this route with organic materials such as dyes [5], poly(vinyl acetate) [6], poly(2-pyridine) [7], poly(vinyl alcohol) [8], and poly(ethyloxazoline) [9] to name a few. The third route to making sol-gel hybrids involves reacting appropriately functionalized (e.g. alkoxysilane functionalized) organic molecules directly into the inorganic network. In doing so, covalent bonds are formed between the organic and inorganic components. Hybrids made by this technique involving low molecular weight organics were first produced by the sol–gel reaction in 1984 and were coined *ormocers* and *ormosils* [10, 11] (“organically modified ceramics” or “silicates”). Similarly, in 1985 the first *ceramer*, composed of poly(dimethyl siloxane) (PDMS) and tetraethoxysilane (TEOS), was reported from our laboratory [12]. The term ceramer is a combination of “ceramic” and “polymer” or “oligomer”. It describes a type of hybrid network system generated from metal alkoxides and functionalized polymers or oligomers (which are not necessarily organic) by the sol–gel reaction. This has remained an active area of research for our group, and some of the research relevant to the current study will be briefly discussed below. More recent sol–gel materials developed in our laboratory include high refractive index hybrid glasses [13], abrasion resistant coatings [14-19], and highly porous

Downloaded At: 12:47 24 January 2011

silica for potential application as a high surface area catalyst or support [20]. An outstanding overall review of the field of hybrid inorganic–organic materials created through sol–gel processing can be found in reference 1, although it is now somewhat out of date. For more recent reviews, see references 21 through 24.

Some of the previous studies from our laboratory focused on hybrid materials made from PDMS with TEOS [25, 26]. One of the complications with synthesizing these ceramers is that the acid catalyst employed in the sol-gel reaction can cause the PDMS chains to undergo chain scission and recombination ("scrambling"), thereby lowering the molecular weight and broadening the molecular weight distribution of the oligomeric PDMS. Another well studied system which avoids this problem is that based on poly(tetramethylene oxide) (PTMO) with TMOS [27-32]. In these materials, however, the PTMO component of the ceramer may crystallize under the proper conditions. The focus of the present work is a new ceramer made from poly(propylene oxide) (PPO) and TMOS. The PPO oligomers used in this study are not stereospecific (atactic), and as such are not crystallizable. The glass transition temperature of high molecular weight PTMO (–84°C [33]) is very close to that of high molecular weight PPO (–78 to –73°C [34-37]), so ceramers made from each with similar formulations are readily comparable. Also, there is no evidence of scrambling of the PPO chains by the acid for the concentrations used in this work. The PPO materials employed in this study are among the class of JEFFAMINE® polyoxyalkyleneamines available from the Huntsman Corporation. These materials are imperfect in their chemistry; they are known to have less than the ideal functionality of two. Recently, Lyondell has brought to the marketplace PPO oligomers (ACCLAIM® polyether polyols) which have very narrow molecular weight distribution and low monol content (and hence nearly ideal functionality). This has led to an interesting comparison of ceramers made from both the JEFFAMINE® and ACCLAIM™ sources, and will be the subject of a later manuscript [38]. The focus of the present report is the influence of the sol–gel variables of water, acid, and TMOS content, as well as the molecular weight of the oligomeric PPO on the final properties of JEFFAMINE® based ceramers. The materials of the present study are comparable to other hybrids previously reported from other laboratories based on similar JEFFAMINEs® (ED2001, ED900, ED600) which are oligomeric forms of ethylene oxide/propylene oxide copolymers [39-42]. These materials are touted to have potential application as optical devices after incorporation of lanthanide cations. Materials similar to these based on oligomeric forms of poly(ethylene oxide) (PEO) and PPO homopolymers have also been

Downloaded At: 12:47 24 January 2011

reported and are considered to be solid electrolytes after incorporation of lithium salts [43-47].

EXPERIMENTAL

Materials and Synthesis

As stated above, the PPO starting materials employed in this study are among the class of JEFFAMINE®s made by the Huntsman Corporation. They are oligomeric forms of linear PPO with *ideally* one primary amine group at the termini of each molecule, that is, they are diamines. Although the JEFFAMINE®s are primarily used as curing agents for epoxies, the reactive amine end–groups may be exploited in many other reactions.

The structure of the JEFFAMINE® materials is shown in Figure 1. The three JEFFAMINE®s employed in this study had the average number of propylene oxide repeat units, n = 2.6, 5.6, and 33.1. They are referred to as D230, D400, and D2000, respectively, the numbers approximately representing the number average molecular weight of the oligomer, and the "D" meaning diamine (ideally). However, the actual functionality of these oligomers is less than 2. The functionality can be calculated based on the primary amine content and average molecular weight provided by the manufacturer, and is listed in Table 1 for

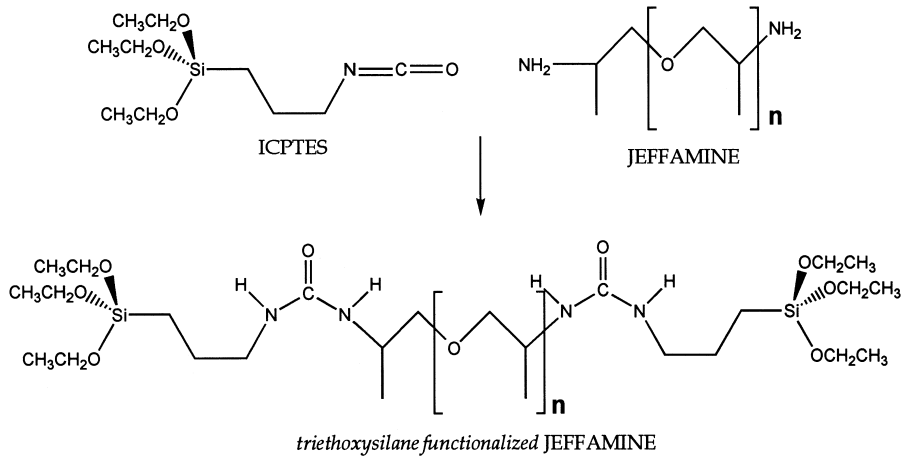

Figure 1. Schematic of the alkoxysilane functionalization of JEFFAMINE® PPO oligomers.

Downloaded At: 12:47 24 January 2011

TABLE 1. Molecular Weight, Breadth Index, and the Average Functionality of the JEFFAMINE® Materials

JEFFAMINE®	n*	$\overline{M}_n$	$\overline{M}_w$	$\overline{M}_w/\overline{M}_n$	f†
D230	≈ 2.6	195	240	1.23	1.89
D400	≈ 5.6	447	494	1.10	1.72
D2000	≈ 33.1	1577	1656	1.05	1.94

* Average number of propylene oxide repeat units.
† Average functionality, i.e. the average number of primary amine groups per molecule (calculated).

Downloaded At: 12:47 24 January 2011

the three JEFFAMINE®s used in this study. Since the functionality of these materials is strictly less than 2, the final network structure of the ceramers is certain to have imperfections such as dangling ends and a notable sol–fraction. Also, the actual number and weight average molecular weights, as well as the breadth indexes, are included in Table 1. These data were graciously provided by the manufacturer, and were measured by gel permeation chromatography (GPC or SEC) in tetrahydrofuran.

Other chemicals used in this study include TMOS (99+%, obtained from Gelest), isocyanatopropyltriethoxysilane (ICPTES, 95%, also from Gelest), isopropanol (IPA, ACS specifications, obtained from EM Science), and 1 M aqueous HCl solution (Aldrich Chemical).

To prepare the PPO oligomers for the sol-gel reaction, they were end-functionalized with alkoxysilane groups through the reaction outlined in Figure 1. The isocyanate moiety on the ICPTES molecule reacts with the amine group(s) on the PPO oligomer to form urea linkage(s). The reaction was carried out at room temperature in 70 wt% solution of IPA, with the isocyanate material (in three mole percent excess of stoichiometry) added dropwise over the course of 15 minutes. Following this addition, the reaction flask was sealed and continuously stirred for eight hours. This forms a new molecular species which can participate in the sol-gel reaction through hydrolysis and condensation of the alkoxysilane end–groups, in the presence of water.

The silane functionalized JEFFAMINE®s can undergo the sol–gel reaction with addition of water and acid catalyst, or may co–react with a metal alkoxide (TMOS in our case) to form a hybrid network as outlined in Figure 2. The

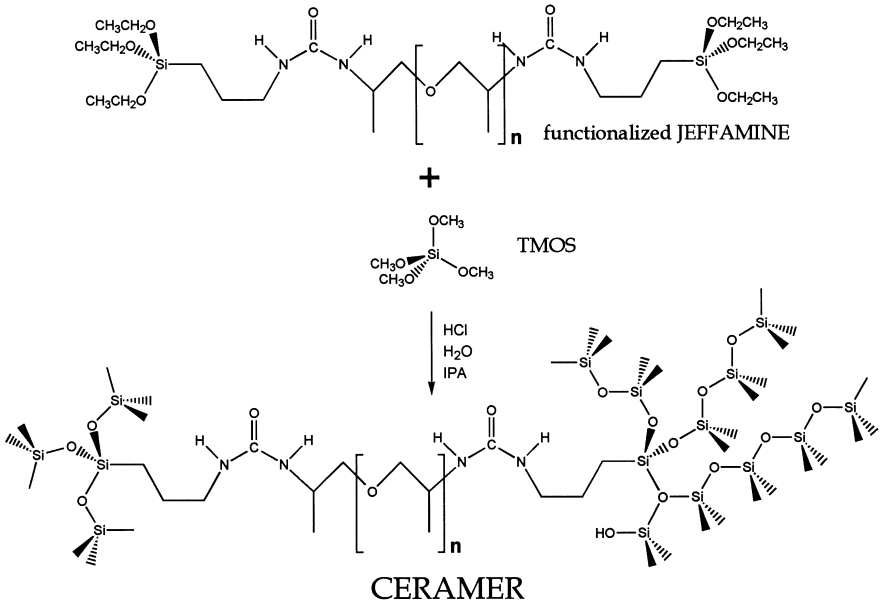

Figure 2. Schematic of the sol–gel reaction of functionalized a JEFFAMINE® PPO oligomer with TMOS.

Downloaded At: 12:47 24 January 2011

sol–gel reaction was carried out by adding to the functionalized JEFFAMINE® (and TMOS if desired) a calculated amount of water and allowing the mixture to stir for ca. one minute. If this reacting liquid was cloudy due to immiscibility of PPO with water, enough IPA was added to clarify the solution and form a homogeneous sol (homogeneous on the scale of the wavelength of visible light). This was followed by the addition of aqueous HCl slowly and dropwise to the briskly stirred beaker. The reaction media was then poured into clean polystyrene petri dishes, degassed in a vacuum chamber, and allowed to cure at room temperature. All samples were aged at laboratory conditions for at least one week prior to testing. The last one or two days of aging was performed under vacuum to remove most of the solvent, by-product alcohols, and water. The small angle X-ray scattering profiles of these ceramer materials remained constant after this aging period, indicating that the reaction reached an equilibrium extent at these curing conditions.

Characterization

All small angle X-ray scattering (SAXS) experiments were performed with nickel filtered, slit collimated Cu$K\alpha$ radiation (1.542 Å [48]) produced by a Philips generator, model PW1729. A Kratky camera and a one–dimensional M. Braun position–sensitive detector were used to collect the scattered radiation. The collimating slit had a width of 100 μm. Absolute intensities were calibrated through the use of a polyethylene (Lupolen) working standard [48]. Parasitic scattering was subtracted from the intensity, however the contribution from thermal density fluctuations has not been removed. Also, the data were not corrected for slit smearing, however desmearing of the SAXS curves would not change our conclusions. The scattering curves were analyzed to yield correlation distances and fractal dimensions where appropriate. SAXS intensity will be plotted versus the magnitude of the scattering vector $s = (2 \sin \theta/\lambda$, where θ is one-half of the radial scattering angle and λ is the wavelength of the radiation (1.542 Å). Correlation distances were determined as the inverse value of s at the location of the interference peaks.

The differential scanning calorimetry (DSC) experiments were performed on a Seiko DSC 220C with nitrogen purge gas. A heating rate of 20 K/min was employed for all scans, and samples weighed between 5 and 10 mg.

Thermogravimetry (TG) was accomplished with a Seiko TG/DTA under air purge. A heating rate of 10 K/min was used and samples weighed between 5 and 10 mg.

A Seiko DMS 210 was utilized for dynamic mechanical spectroscopy (DMS) experiments. Rectangular samples had a gauge length of 10 mm, and were cut such that their cross–sectional area was between 2 and 7 mm^2. Scans were started at room temperature, and cooled slowly (1.5–2 K/min) with liquid nitrogen to ≈ –150°C while collecting data. After this cooling scan, the sample was allowed to equilibrate back to room temperature, and a heating scan was then started under nitrogen purge gas with a heating rate of 1.5–2 K/min. The data from the heating and cooling scans were then combined to give the thermomechanical spectrum for each sample. All DMS data shown in this report were measured at an oscillation frequency of 1 Hz.

Samples were extracted with acetone in an extraction thimble until the resulting values of the sol fraction did not change with time. The extraction thimble is a glass vial with a porous frit. It is placed in a beaker of solvent, enough to entirely submerge the sample but not the vial. The porous frit allows solvent and extracted material to pass, while retaining the network film.

Downloaded At: 12:47 24 January 2011

Complete extraction generally took one week, while removing old acetone and adding fresh every few days. The measurement process involved weighing the sample and extraction vial before the experiment. After exposure to the extracting solvent, the vials and extracted samples were dried by vacuum chamber for several days before weighing. All steps in the extraction process were performed at laboratory temperature.

Nomenclature

Due to the numerous variables explored in this work, a simplified system of nomenclature has been employed so that samples can be easily differentiated. This will be illustrated by the following example:

f-D2000(50) TMOS(50) 4/1/0.02

The f-D2000(50) represents alkoxysilane end–functionalized JEFFAMINE® D2000 which is 50 wt% of the initial reaction mixture (relative to TMOS content). The TMOS(50) represents 50 wt% tetra-methoxysilane, and the 4/1/0.02 represents the molar ratio of water/alkoxy-silane/HCl employed during the sol–gel reaction. The combined weight percent of the functionalized JEFFAMINE® and the TMOS always adds up to 100 wt% for all formulations.

Downloaded At: 12:47 24 January 2011

RESULTS AND DISCUSSION

For reference, a few of the basic properties of various ceramers of the 4/1/0.04 formulation have been archived in Table 2. These include glass transition temperatures, silicate contents, sol fractions, correlation lengths, and fractal dimensions. All of these properties will be examined in further detail with respect to each formulation variable.

Influence of Water Content

f-D2000(100) Ceramers

A strong peak is observed in the SAXS data for all ceramers of the f-D2000(100) family (Figure 3 which shows both the varied water and acid content). This peak corresponds to a microphase separated structure, where the oligomeric PPO chains form the continuous phase, segregated from the dispersed silicate phase, which provides significant contrast in electron density on the scale

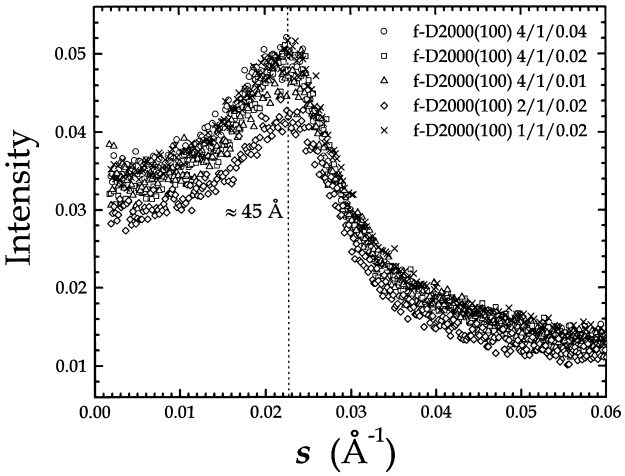

Figure 3. The influence of water and acid content on the SAXS behavior of f-D2000(100) ceramers.

Downloaded At: 12:47 24 January 2011

of the X-ray wavelength. For the three SAXS curves of varied water content labeled 4/1/0.02, 2/1/0.02, and 1/1/0.02, all have the same correlation length (Bragg spacing) near 45 Å. Hence, water does not significantly influence the phase separated structure of the final networks for the range probed. This is reinforced by the DSC data of Figure 4. Again across the same variation in water content, all DSC scans show a clear glass transition at –56°C, corresponding to

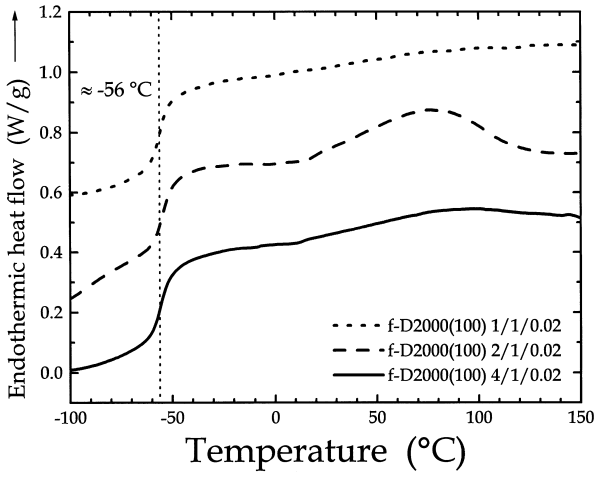

Figure 4. The influence of water content on the DSC scans of f-D2000(100) ceramers. Scans displaced vertically for clarity.

the glass transition of the phase separated PPO chains. Pure, high molecular weight PPO homopolymer has a reported [34-37] dilatometric glass transition temperature in the range of –78 to –73°C. The presence of endothermic "bumps" in the range of 40 to 120°C of Figure 4 is likely due to the release of water, solvent, and by-product alcohols. This has been confirmed by the absence of such bumps in a second heating scan of the same sample. There is no clear trend in the appearance of these bumps as a function of water content. There is a very slight weight loss (0.4%) in this temperature range in the TG data (not shown). This TG data for the series of varied water content also show no significant deviation in behavior.

The dynamic mechanical data similarly show that the water content plays a relatively insignificant role in the final properties as seen in Figure 5 (varied water and acid content included in this plot). For the three water contents probed here, all materials have an identical glass transition (≈ –57°C), and the thermomechanical spectra essentially coincide. Hence the mechanical behavior is also unaffected by the water content for the range probed here.

For these f-D2000(100) materials, the storage modulus in the glassy state is ≈ 6 GPa, and drops roughly three orders of magnitude across the glass transition into the rubbery state. This behavior is also characteristic of isotropic, amorphous, organic polymers, as well as unfilled, *lightly* crosslinked organic networks.

Downloaded At: 12:47 24 January 2011

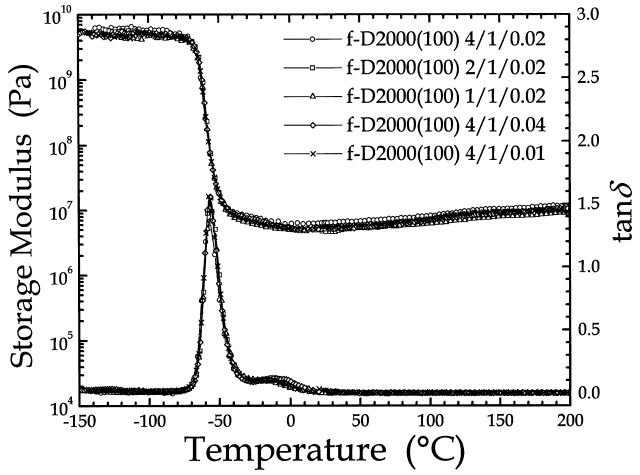

Figure 5. The influence of water and acid content on the thermomechanical spectrum of f-D2000(100) ceramers.

The storage modulus for these materials in the temperature range of 25 to 200°C (rubbery plateau) displays a slight increase with temperature. This may be due to further reaction above room temperature (which was the original cure temperature), thereby increasing the crosslink density and hence the modulus. Another explanation would be the rubber elastic effect. From ideal rubber elasticity it can be shown that [49]:

$$G = N_v kT = \frac{\rho RT}{M_c} = \frac{1}{3}E \tag{1}$$

G is the shear modulus and E is Young's modulus, both of which are determined from equilibrium experiments, not dynamic oscillatory measurements (which the storage modulus, E' is determined from in Figure 5). Regardless of the dynamic mechanical data being non-equilibrium data, it has been observed that such dynamic experiments provide results which are compliant with equilibrium swelling measurements for similar hybrid systems based on PTMO and TEOS [50]. Continuing discussion of equation (1), N_v is the number of crosslinks per unit volume, k is Boltzmann's constant, T is the absolute temperature, ρ is the bulk density, R is the universal gas constant, and M_c is the number average molecular weight between crosslinks. Although Equation 1 is for the equilibrium modulus, the dynamic storage modulus is still expected to have the similar dependence on temperature in the rubbery state, i.e., (this proportionality to temperature is considered the rubber elastic effect). It then follows that, for a material that obeys ideal rubber elasticity, knowledge of the modulus E_1 at a given temperature T_1 can be used to calculate the modulus of that material E_2 at temperature T_2 (assuming the density change from T_1 to T_2 is negligible) by the following:

$$E_2 = E_1 \frac{T_2}{T_1} \tag{2}$$

This is analogous to using the perfect gas law for calculating the pressure P_2 of a gas at some temperature T_2 given the knowledge of the pressure P_1 at T_1 for an isochoric process. Applying this approach to the data in Figure 5 within the rubbery plateau, the modulus values thus predicted by rubber elasticity are lower than the measured values. Hence, the increase in storage modulus with temperature in the range of 50 to 200°C is believed to be due to a combination of the rubber elastic effect (T increasing in Equation 1) and the increasing crosslink density due to further reaction above room temperature (N_v increasing or M_c decreasing in Equation 1). This can be confirmed by annealing a sample at an elevated temperature and afterward measuring the thermomechanical spec-

Downloaded At: 12:47 24 January 2011

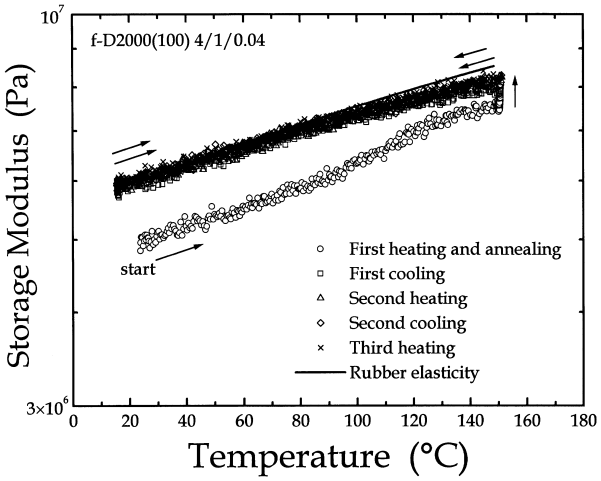

Figure 6. A cyclic dynamic mechanical experiment in the rubbery region of f-D2000(100) 4/1/0.04. The first heating scan shows the combined influence of the rubber elastic effect and increasing crosslink density (further reaction) on the storage modulus. However, after annealing at 150°C for 1 hour, the subsequent cooling and heating scans illustrate only the rubber elastic effect.

Downloaded At: 12:47 24 January 2011

trum in the rubbery region. This has been achieved Figure 6, where a sample of f-D2000(100) 4/1/0.04 was heated from room temperature to 150°C, annealed there for 60 minutes, cooled back to room temperature, and reheated to 150°C, collecting data along the way for each step. The storage modulus data collected during the first heating is curved upward as temperature is increased (just as the data in Figure 5), and annealing at 150°C causes a continued increase. However, the data from the subsequent cooling and heating steps all coincide. The line which has been drawn in the figure, which closely follows the subsequent cooling and heating data at the lower temperatures (15 to 70°C), represents the proper shape for ideal rubber elasticity (calculated by Equation 2). The experimental data lie a bit below the rubber elasticity line at higher temperatures, likely due to the presence of loose chains (sol–fraction). From Table 2, it can be seen that this ceramer has a sizable sol–fraction in the amount of 5.6 wt% of the total sample. Hence, Figure 6 confirms that upon the initial heating step of the DMS experiment, further curing occurs, leading to an increased crosslink density. This generates higher storage modulus values during the first heating scan than is to be expected purely from the rubber elastic effect.

TABLE 2. Glass Transition, Silicate Content, Sol Fraction, Correlation Length, and Fractal Dimension Data for Various Ceramers of the 4/1/0.04 Formulation

sample	T_g* (°C)	silicate content† (wt.%)	sol fraction (wt.%)	correlation length (Å)	fractal dimension‡
f-D2000(100)	−57	13	5.6	45	–
f-D2000(75) TMOS(25)	−46	22	2.9	–	2.7
f-D2000(50) TMOS(50)	−23	36	0.8	–	2.5
f-D400(100)	17	31	1.3	29	–
f-D230(100)	36	34	–§	25	–

* Determined from DMS data as the midpoint of the drop in storage modulus across the glass transition.

† Estimated from char yield measured by TG.

‡ Slit-smeared SAXS result.

§ Not measured.

Downloaded At: 12:47 24 January 2011

Interestingly, a small shoulder is observed in the tan δ data just above the main glass transition in Figure 5. This relaxation process will be addressed in the section concerning the influence of TMOS content.

f-D2000(50) TMOS(50) Ceramers

The influence of water concentration on the properties of TMOS containing ceramers is likewise trivial. However, there is a noticeable difference in the SAXS curves for f-D2000(50) TMOS(50) ceramers of varied water content, as shown in Figure 5. The material with the least water content, the 1/1/0.02 ceramer, has a distinct peak at 59 Å. Doubling the water concentration (the formulation of 2/1/0.02) leads to a slightly increased spacing of 61 Å. This may not be a significant difference. The sample of 4/1/0.02 formulation, however, shows a clearly different SAXS pattern, as a shoulder rather than a peak is observed. This shoulder appears at a lower angle than that corresponding to 61 Å.

The plot on the right in Figure 7 is a double log presentation of the data on the left. In this presentation, the mass fractal character of the ceramer materials can be discerned. This is evidenced by the linear shape in the tail portion (Porod region) of the plot. For a material to be truly fractal, this linear region must be maintained over at least one decade of *s*, which is not accomplished here [32]. However, if the data could be collected to wider angles than the current

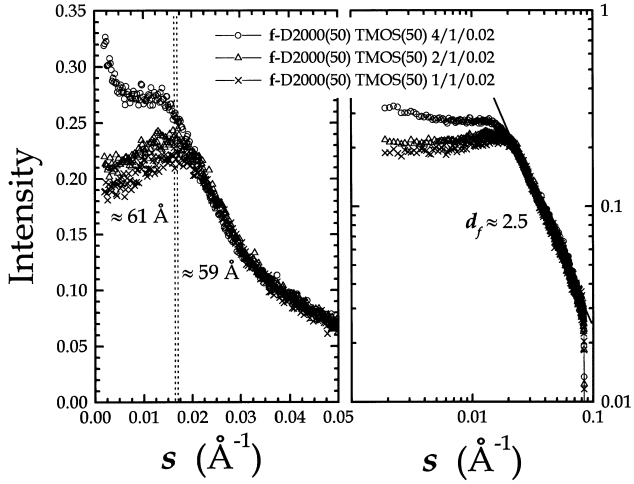

Figure 7. The influence of water content on the SAXS behavior of f-D2000(50) TMOS(50) ceramers. Plot on right is a double–log presentation of the same data in the plot on the left, which brings out the mass fractal character of these ceramers.

Downloaded At: 12:47 24 January 2011

instrument allowed, this linear behavior might continue. Nevertheless, it has been suggested that trends can certainly be recognized using data which covers less than one decade [32]. The slope within the Porod region is related to the fractal dimension. The relationship depends on the type of fractal (mass or surface) and the form of X-ray beam collimation. All of the fractal ceramers studied here were mass fractals. For such materials, the mass (M) of the object scales with the characteristic length to the power of the fractal dimension (d_f): $M \propto (length)^{df}$. Since slit collimation was employed throughout this work, the relationship between the Porod slope (m) and the fractal dimension is $d_f = 1 - m$. For pin–hole collimation, $d_f = - m$; other details concerning fractals have been discussed elsewhere [32, 51-53]. The two ceramers with the lower water content (1/1/0.02 and 2/1/0.02) both possess a peak on the plot (as they did in the log–log plot of Figure 7, although not easily seen in the figure), followed by a linear region indicative of a fractal.

It should be noted that in these materials which possess a clear correlation peak, the Porod region may contain a contribution to the scattered intensity from a second order of the main correlation peak. This would influence the slope in the Porod region and hence the value of the fractal dimension may be incorrectly measured. This point is duly noted, and such data is analyzed for trends only.

The highest water content ceramer (4/1/0.02) has no distinct peak, but the fractal character is easily seen. The approximated fractal dimension for all three materials is roughly the same, ≈ 2.5. This means that the mass of these ceramers scales with its length to the power of 2.5. A solid, three-dimensional object of uniform density would have fractal dimension = 3. Hence, the molecular structure here is somewhat more "open", or less space filling, than a uniform solid. Although the fractal dimension appears to be independent of water concentration for this series of f-D2000(50) TMOS(50) ceramers, the scattering curves are quite different when plotted on a linear scale as discussed above.

The thermomechanical spectra of these TMOS containing ceramers show no significant effect of water content as shown in Figure 8. The three spectra in this plot coincide. The glass transition is broader (onset ≈ –60°C, end point ≈ 70°C) and at a higher temperature (≈ 10 °C) than the corresponding materials made without TMOS. The extreme broadness of the glass transition is due to a widely varied environment which the PPO chains inhabit. Some regions exist which are predominantly rich in PPO chains, and this would correspond to the lower temperature portion of the transition region. With 50 wt% TMOS available during the sol-gel reaction, some regions likely exist where the PPO chains are highly constrained by an abundance of dense silicate structure. This would correspond to the higher temperature portion of the glass transition region. In between these two extremes, a distribution of structures exists which would lead

Downloaded At: 12:47 24 January 2011

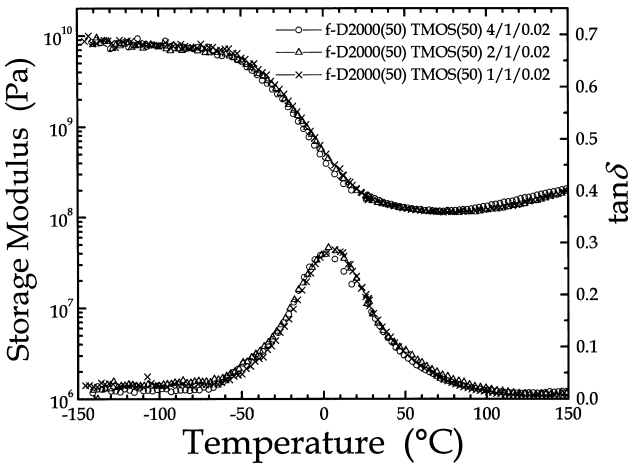

Figure 8. The influence of water content on the thermomechanical spectra of f-D2000(50) TMOS(50) ceramers.

to the observed broadness of the glass transition. A more detailed discussion is to follow in the section concerning the influence of TMOS content.

Also, the tan δ data of the 4/1/0.02 formulation shows a small shoulder at the low temperature end of the glass transition, near –50°C. Again, this is due to the PPO chains which are most sharply phase separated and free of excessive constraints by the silicate material. This shoulder is less noticeable in the 2/1/0.02 material and is not present in the 1/1/0.02 formulation. It is hypothesized that this shoulder is due to the low miscibility of the D2000 material in water. Hence, even though the reacting sol appears homogeneous (on the scale of the wavelength of visible light), this high water content formulation is likely to lead to a sharper phase separation of a portion of the PPO chains in the final network, when compared to a formulation with less relative water content (and more relative IPA). This sharper phase separation would lead to higher contrast in electron density (this contrast is a necessary component of the scattering power of a material). This is in agreement with the observation in the SAXS data of Figure 7 that the integrated intensities increase with increasing water content (and hence the materials are increasing in scattering power due to sharper phase separation).

Downloaded At: 12:47 24 January 2011

One last consideration of the dynamic mechanical data is that the storage modulus in the glassy state for these materials is roughly 10 GPa, and drops only 2 orders of magnitude across the glass transition into the rubbery state. This behavior is characteristic of a filler-reinforced elastomer and also a more highly crosslinked network. This issue will be discussed in more detail in the section on the influence of TMOS content.

The DSC scans for these three TMOS containing ceramers similarly show a very broad glass transition temperature, centered around ≈ –25°C (not shown for brevity). The onset temperature appears to be near –60°C, and the endpoint near 15°C. Admittedly, the glass transition temperatures are difficult to discern by DSC; the DMS technique is much more sensitive for this purpose. The low sensitivity of the DSC technique is primarily due to the relatively low mass fraction of PPO in these ceramers. Again, some endothermic bumps are present in the DSC scans at elevated temperatures (≈ 100°C and above) which, as stated earlier, are believed to be due to the release of water, solvent, and by-product alcohols.

Influence of Acid Content

Since acid is a catalyst for the sol-gel reaction, increasing its concentration is expected to increase the sol-gel reaction rate, and hence reduce the gel time for a given formulation.

f-D2000(100) Ceramers

As with the series of varied water content, the SAXS curves for the family of f-D2000(100) ceramers of varied acid content all possess a peak at ≈ 45 Å, shown in Figure 3. The five curves of varied acid and water content essentially coincide, implying that the acid content also has no influence on the structure observed by SAXS. This is supported by the dynamic mechanical spectra of Figure 5. Again the five spectra corresponding to varied acid and water content coincide. DSC provides supporting evidence (not shown) that acid content has no effect on the final properties of the f-D2000(100) ceramers within the range probed. All three scans show a clear glass transition at ≈ –56°C, just as the materials in Figure 4.

f-D2000(50) TMOS(50) Ceramers

The SAXS profiles for the f-D2000(50) TMOS(50) materials do exhibit a dependence on acid content, as shown in Figure 9. The lowest acid content ceramer (4/1/0.01) shows a small peak at ≈ 76 Å. Increasing the acid content leads to a transition of the peak into a shoulder. The highest acid content material (4/1/0.04) shows a very slight shoulder, with no distinct correlation length in Figure 9. Plotting the SAXS data on a double–log scale in the graph on the right again brings out the fractal character of these ceramers. The fractal dimension for these three materials are all in the range of 2.4 to 2.6, with no obvious trend with acid concentration.

Downloaded At: 12:47 24 January 2011

There is also a noticeable difference in the thermomechanical spectra for this series, as shown in Figure 10. The peak observed in the tan δ data for the lowest acid content material (4/1/0.01) occurs over the broadest temperature window. The extreme broadness of the glass transition is again due to the widely varied environments that the PPO chains inhabit. The peak of the "main" relaxation for this material occurs at ≈ 10°C, and a small shoulder is present at ≈ –50°C. There also appears to be a small shoulder in the higher temperature near 90°C.

The 4/1/0.02 formulation has a slightly less broad glass transition, and the peak of the main relaxation appears at a slightly lower temperature (≈ 0°C) than the lowest acid content formulation. However, an equivalent low temperature shoulder is present at ≈ –50°C. The high acid content ceramer (4/1/0.04) displays the lowest temperature main relaxation, at ≈ –15°C. The low temperature shoulder is present for this material as well. There is a second shoulder apparent for this material above the main glass transition, near 100°C.

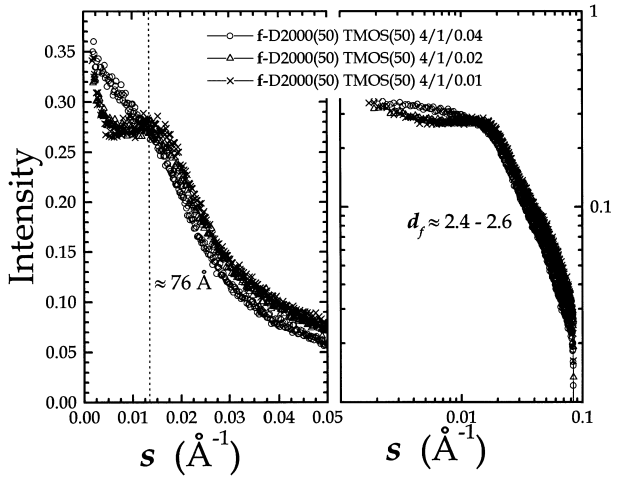

Figure 9. The influence of acid content on the SAXS behavior of f-D2000(50) TMOS(50) ceramers. Plot on right is a double–log presentation of the same data in the plot on the left, which brings out the mass fractal character of these ceramers.

Downloaded At: 12:47 24 January 2011

For this series of materials the DSC again proves to be a much less sensitive probe than DMS (not shown). All three samples appear to have similar glass transition temperatures, near ≈ –30°C by this method, and are very broad and their location is difficult to pinpoint.

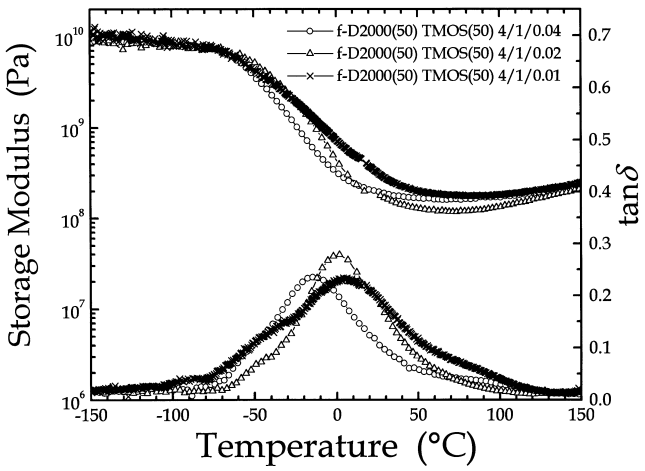

Figure 10. The influence of acid content on the thermomechanical spectra of f-D2000(50) TMOS(50) ceramers.

Downloaded At: 12:47 24 January 2011

Influence of TMOS Content

The addition of TMOS to the PPO based ceramers leads to a drastic change in morphological structure. This is easily seen in the SAXS data of Figure 11 which shows the scattering curves for f-D2000(100), f-D2000(75) TMOS(25), and f-D2000(50) TMOS(50), all of the formulation 4/1/0.04. The sample with no added TMOS, the f-D2000(100) ceramer, has a distinct peak as noted before at 45 Å. However the sample with only 25 wt% TMOS has a shoulder with no distinct peak. Incorporation of 50 wt% TMOS leads to a very broad shoulder. The integrated intensity also increases with increasing TMOS content (in this range of 0-50 wt%), or rather, the *invariant* increases with TMOS content. To describe this observation, a brief discussion of the scattering power and the invariant will be necessary. The invariant Q_s can be expressed as [48]:

$$Q_s = \int_0^\infty s \cdot I(s)\, ds \tag{3}$$

for slit–smeared absolute intensity $I(s)$. The invariant is related to the mean square fluctuation in electron density $\langle \Delta\rho^2 \rangle$ (or scattering power) which, for a two phase system displaying sharp phase separation, where each phase is of uniform electron density, the following simplified mathematical relationship holds:

$$\left\langle \Delta\rho^2 \right\rangle = \phi_{PPO} \cdot \phi_{sil} \cdot (\rho_{PPO} - \rho_{sil})^2 \;\propto\; Q_s \tag{4}$$

By employing this equation, we are assuming that the ceramers are two phase systems, composed of a PPO phase of volume fraction ϕ_{PPO} and electron density ρ_{PPO}, and a separate silicate phase of volume fraction $\phi_{sil} = 1 - \phi_{PPO}$, and electron density ρ_{sil}. With the value of remaining constant, $\langle \Delta\rho^2 \rangle$ reaches a maximum at $\phi_{PPO} = \phi_{sil} = 0.5$. Hence the trend of increasing integrated intensity with increasing TMOS content (approaching 0.5 volume percent) of Figure 11 is certainly expected. Note that the infinite integral of Equation 3 has not actually been evaluated for the data here. However, one can visually rank the area under the SAXS curves, since the curves for each sample do not crossover at any point for the range of s measured in this study (measurements went to $s = 0.08$ although the plot displays only up to $s = 0.05$).

As can be seen in the double–log plot of this SAXS data on the right in Figure 11, adding TMOS to the f-D2000 ceramer formulation leads to a more mass fractal material. That is to say, the linearity in the Porod region extends over a larger range of s as the TMOS content is increased up to 50 wt%.

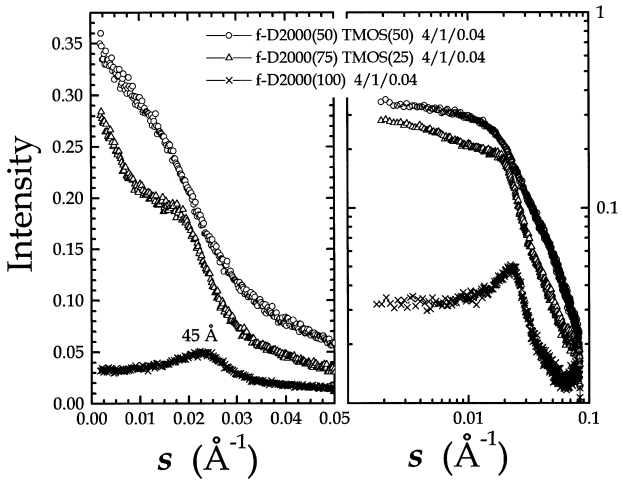

Figure 11. The influence of TMOS content on the SAXS behavior of f-D2000 based ceramers. Plot on right is a double–log presentation of the same data in the plot on the left, which brings out the mass fractal character of these ceramers.

Downloaded At: 12:47 24 January 2011

There is also a drastic difference in the dynamic mechanical behavior of the varied TMOS containing ceramers, as shown in Figure 12. Although all three samples show virtually the same storage modulus in the glassy region, at and above the glass transition, the material behaviors diverge. The glass transition, as ascertained from the storage modulus data, increases and broadens with increasing TMOS content. The f-D2000(100) ceramer behaves similarly to an amorphous, lightly crosslinked organic network in that there is a three order–of–magnitude decline in the storage modulus across the glass transition, noted earlier. However, the presence of the silicate phase derived from TMOS in the other two materials greatly increases the storage modulus in the rubbery region. Similar behavior has been noted in elastomers which contain a reinforcing filler [54] in some cases an increase and broadening in the glass transition has been observed [55, 56]. Here the reinforcing filler is the silicate phase. More interesting information can be uncovered by examining the tan δ data, to be addressed next.

For the f-D2000(100) ceramer, the PPO chains are crosslinked by the silicate solely at the two ends of each linear molecule. Therefore, between each silicate crosslink junction is a $\approx$ 2000 g/mol PPO chain (along with the urea and n-propyl groups). This can be envisaged as a long rope held rigidly at both ends,

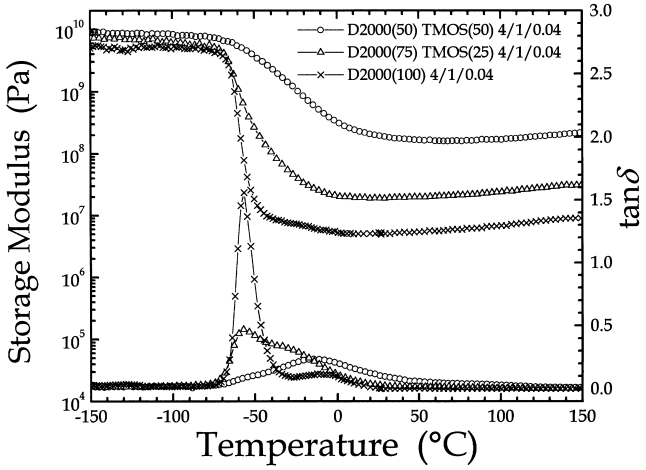

Figure 12. The influence of TMOS content on the thermomechanical spectra of f-D 2000 based ceramers.

Downloaded At: 12:47 24 January 2011

where the rope has a coil–like conformation in between. PPO segments which are farthest from both crosslinked silicate ends are the most mobile, (like the bulk of the rope far from the held ends) and hence have the lowest glass transition near that of homopolymeric PPO. This is the relaxation which is observed in the tan δ data in Figure 12 at –55°C. Segments near the silicate ends are highly *constrained on this end*, but are much more free in the opposite direction which consists of other PPO segments (this is like the region of the rope near a grasped end). Ethylene oxide segments near the silicate clusters of a similar PEO ceramer have been shown to have lower mobility than segments farther from the rigid silicate particles [57, 58]. The *partially constrained* PPO segments in the present material are one possible source of the small peak at –10°C, just above the main relaxation. The magnitude of the relaxation of these partially constrained segments is considerably smaller than the magnitude of the major glass transition at –55°C due to their lower concentration when compared to the more mobile, homopolymeric–like PPO segments. Although the subject of a subsequent report [38] ceramers made from the ACCLAIM™ polyether polyol of a similar formulation also possess a small relaxation above the main glass transition. For these ACCLAIM™ ceramer materials, this relaxation appears as a shoulder to the main relaxation rather than a distinct peak as seen for the JEFFAMINE® systems. Such a shoulder has been observed (although not dis-

cussed) for other ceramer systems such as ones based on hydrogenated polybutadiene (Figure 12 of reference 59). This sort of post–T_g relaxation process is also likely due to segments at the interface between the silicate phase and the PPO phase. This is often referred to as an *interphase*, which for the various ceramer materials addressed above, likely contains the linking urea or urethane groups.

When 25 wt% TMOS is added to the formulation, the resulting silicate phase can interact with the PPO segments at locations other than just the PPO chain ends. Therefore, the rope analogy becomes too simplistic to describe the types of environment in which the PPO chains may inhabit. Expectedly then, the magnitude of the relaxation of the mobile, homopolymeric–like PPO segments (at –55°C) decreases in Figure 12 for the 25 wt% TMOS sample [27] (compared to the f-D2000(100) sample). This is accompanied by the appearance of a distribution of relaxation processes at higher temperatures, resulting from these other silicate–PPO interactions.

Downloaded At: 12:47 24 January 2011

When 50 wt% TMOS is incorporated, the low temperature, homopolymeric–like PPO relaxation becomes a small shoulder rather than a peak (Figure 12). Hence the concentration of unconstrained PPO segments in this f-D2000(50) TMOS(50) ceramer is very small. Similar to the 25 wt% TMOS sample, a distribution of higher temperature relaxation processes exists in this material. The tan δ peak for the 50 wt% TMOS ceramer reaches a higher temperature than the 25 wt% TMOS material, due to the increased constraints imposed by the greater amount of silicate in this sample.

A critical point to mention is the poor tensile stress–strain properties of these JEFFAMINE® based ceramers. The sample–to–sample variation was rather great, and the samples generally failed at very low values of strain ($\varepsilon_b < 0.15$). The shape of the σ_0–ε curves were linear, like that of a Hookean spring. This behavior of low strain at break and Hookean shape was observed for similar ceramers based on PDMS and TEOS [60, 61]. This is in contrast to the superior tensile behavior of similarly formulated ceramers based on the ACCLAIM™ poly(propylene oxide) oligomer, which as stated earlier, is the subject of a subsequent paper [38].

The DSC data for this series of materials is shown in Figure 13. It can be seen from this figure that increasing the TMOS content leads to a higher and broader glass transition, which directly supports the DMS data. The f-D2000 (100) material has the largest change in heat capacity across the glass transition, ΔC_p, which is expected in light of the relative weight fraction of PPO in this material is the highest of the three samples.

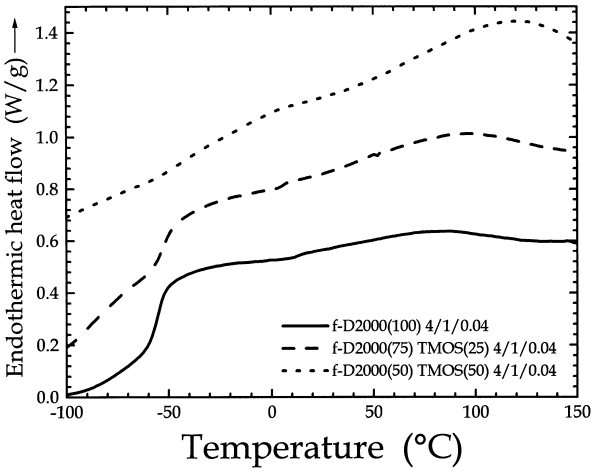

Figure 13. The influence of TMOS content on the DSC scans of f-D2000 based ceramers. Scans displaced vertically for clarity.

Downloaded At: 12:47 24 January 2011

The TG data of Figure 14 was employed to estimate the weight fraction of silicate in the ceramer (values listed in Table 2). Assuming that the remaining material at the end of the scan ("char yield") is only the inorganic silicate component and all of the organic material was pyrolyzed, the char yield can be utilized as a rough estimate of the silicate content in the original ceramer. The silicate component for the f-D2000(100) material is generated solely from the alkoxysilane groups at the chain ends of the f-D2000 material as no metal alkoxide was added to this formulation. A simple calculation shows that the alkoxysilane end–groups of the f-D2000 represent 13% of the total molecular weight of the f-D2000 molecule (before the sol-gel reaction). However, in the network ceramer it is expected that a large portion of the alkoxysilane groups would be condensed, liberating water and alcohol; if the alkoxysilane groups were completely condensed, these end–groups (—$SiO_3 \equiv \equiv$) would correspond to 7 % of the total weight of one "fully condensed f-D2000 molecule." The char yield then is expected to lie between 7 and 13 wt% for the f-D2000(100) ceramer. A small amount of the measured char yield (13%) may be due to carbonized organic material left behind and trapped inside the network oxide. As anticipated, adding TMOS to the formulation leads to an increase in the char yield (and hence, silicate content) of the final material; f-D2000(75) TMOS(25) has 22 wt% char yield and f-D2000(50) TMOS(50) has 36 wt% char yield. Note that TMOS

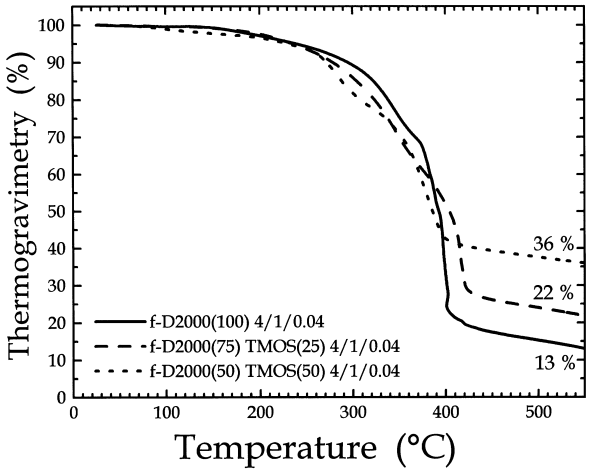

Figure 14. The influence of TMOS content on the thermogravimetry of f-D2000 based ceramers.

Downloaded At: 12:47 24 January 2011

ejects a large portion of its mass upon hydrolysis and condensation (lost as methanol and water), and therefore, the silicate content in the TMOS containing ceramers is lower (for the range probed here) than the weight fraction of TMOS added to the sol-gel reaction.

Influence of PPO Molecular Weight

The molecular weight of the PPO chains also plays a major role in the behavior of these ceramer materials. This variable will be discussed for non–TMOS containing samples only. The variation in the morphological structure can be seen in the SAXS profiles of Figure 15 (not absolute intensity). All three samples possess a correlation length, which increases with the initial oligomer molecular weight. Increasing the molecular weight increases the average end–to–end distance of the PPO chains, and hence the correlation distance increases accordingly [31, 42]. Also, the sharpness of the peak increases with molecular weight. This is due to the sharper phase separation of the higher molecular weight PPO chains, or conversely the improved incorporation and compatibility of the lower molecular weight PPO chains with the silicate component. This has been observed for PDMS–TEOS ceramers [26] as well as PTMO–TEOS ceramers [32] and is supported by the following dynamic mechanical data.

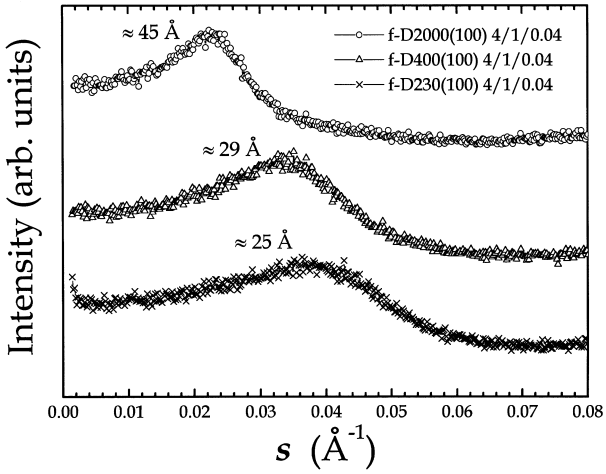

Figure 15. The influence of PPO molecular weight on the SAXS behavior of non-TMOS containing ceramers. Intensities are not absolute and the curves are displaced vertically for clarity.

Downloaded At: 12:47 24 January 2011

Figure 16 shows the influence of PPO molecular weight on the thermomechanical spectra of this series of samples. Decreasing the PPO molecular weight leads to an increased and broadened glass transition. The two lower molecular weight PPO oligomers (f-D400 and f-D230) do not exhibit a relaxation corresponding to the homopolymeric–like PPO segments which the f-D2000 ceramer has. Since these shorter PPO chains have on average 5.6 and 2.6 propylene oxide repeat units respectively, the lack of a homopolymeric–like relaxation is expected. Hence the short chains are highly constrained at both ends, without a free, coil–like structure in between. With the shorter PPO chains, the relative amount of silicate is greater due to the increased concentration of alkoxysilane end–groups. This is confirmed by the TG data of Figure 17, the results of which are included in Table 2. Hence, decreasing the JEFFAMINE® molecular weight has a similar effect of increasing the TMOS content. Not surprisingly then, the relaxation processes observed in f-D400(100) and f-D230(100) of Figure 16 are broadened compared to the f-D2000(100) ceramer due to this large amount of silicate present, which can easily constrain the motions of the PPO segments. Broadening is likely aided by the presence of dangling ends, which are mostly a result of the imperfect functionality (<2) of the starting JEFFAMINE® materials. The dangling ends would relax at a lower temperature since they are only con-

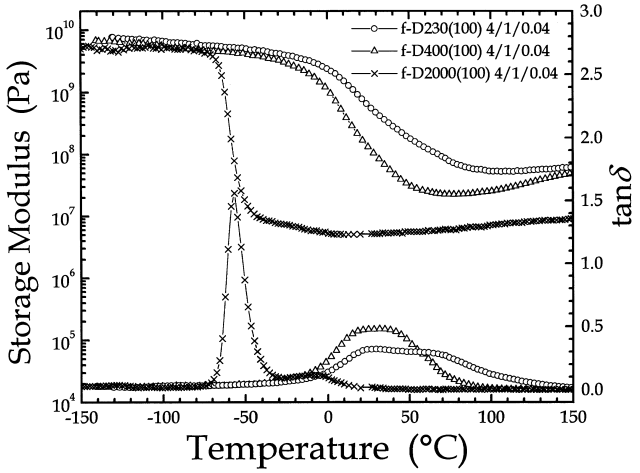

Figure 16. The influence of PPO molecular weight on the thermomechanical spectra of non-TMOS containing ceramers.

Downloaded At: 12:47 24 January 2011

strained at one chain end. Also broadening would be enhanced by the distribution of molecular weight of the starting JEFFAMINE® materials, as the D230 has the broadest molecular weight distribution and the D2000 has the narrowest (Table 1).

Lastly, the DSC curves for this series of ceramers are shown in Figure 18. Again these data support the DMS results. As the PPO molecular weight

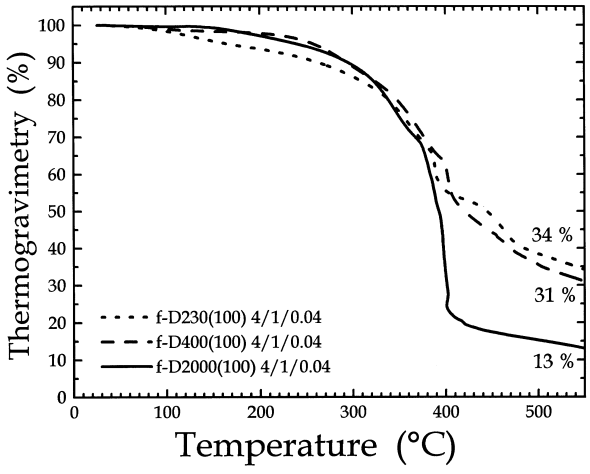

Figure 17. The influence of PPO molecular weight on the TG of non-TMOS containing ceramers.

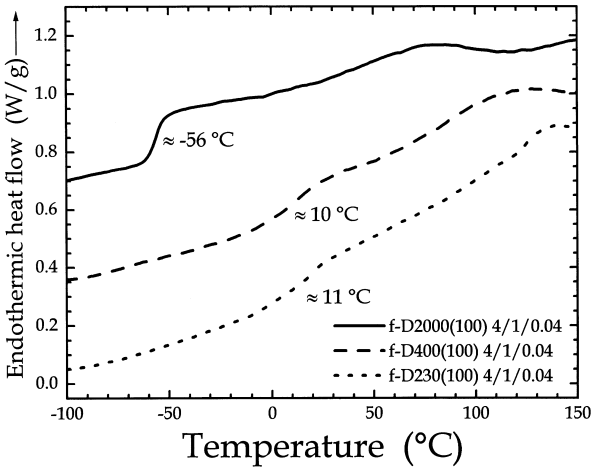

Figure 18. The influence of PPO molecular weight on the DSC scans of non-TMOS containing ceramers. Scans displaced vertically for clarity.

Downloaded At: 12:47 24 January 2011

decreases, the glass transition increases and broadens, for reasons discussed above, and decreases due to the reduction in the relative weight fraction of PPO in the ceramer.

CONCLUSION

For the novel ceramers synthesized in this study based on JEFFAMINE® PPO oligomers and TMOS, the following conclusions can be made:

Both the water and acid concentration have little influence on the final properties of our ceramers for the ranges probed in this study. However, increasing the water content for f-D2000(50) TMOS(50) ceramers lead to sharper phase separation of the PPO chains from the silicate due to the immiscibility of PPO with water.

Increasing the TMOS content has a similar effect as decreasing the PPO molecular weight; both lead to an increased and broadened glass transition. This is due to an increase in the relative amount of silicate material which behaves like a reinforcing filler. Furthermore, decreasing the PPO molecular weight decreases the average molecular weight between crosslinks. This phenomenon also has the effect of increasing the glass transition temperature.

Increasing the TMOS content tends to promote a more mass fractal structure for the f-D2000 based ceramers of 4/1/0.04 formulation.

Increasing the PPO molecular weight increases the correlation length for non–TMOS containing ceramers observed by SAXS. This is expected since increasing the PPO chain length expands the average distance between the crosslinking silicate end–groups.

Increasing PPO molecular weight also leads to a sharper phase separated structure due to the general decrease in miscibility with increasing molecular weight.

DMS has proven to be a very sensitive instrument to probe the structure and thermal transition behavior of these ceramers, whereas DSC was rather insensitive.

Downloaded At: 12:47 24 January 2011

ACKNOWLEDGEMENTS

The authors wish to thank the Huntsman Corporation for generously supplying the JEFFAMINE® polyoxyalkyleneamines for this study. We would also like to thank specifically Debra Direnfeld of the Huntsman Corporation for providing the molecular weight data for the JEFFAMINE®s employed in this study.

REFERENCES

[1] C. Sanchez and F. Ribot, *New J. Chem., 18,* 1007 (1994).

[2] J. D. Mackenzie, Y. J. Chung, and Y. Hu, *J. Non-Cryst. Solids, 147 and 148,* 271, (1992).

[3] E. J. A. Pope and J. D. Mackenzie, *Mater. Res. Soc. Bull., 12,* 29, (1987).

[4] B. Abramoff and L. C. Klein, in *Sol–Gel Optics I,* J. D. Mackenzie, D. R. Ulrich, Eds., *Proc. SPIE, 1328,* 241 (1990).

[5] D. Avnir, D. Levy, and R. Reisfield, *J. Phys. Chem., 88,* 5954 (1984).

[6] C. J. T. Landry and B. K. Coltrain, *Am. Chem. Soc. Div. Polym. Chem. (Polymer Preprints), 32,* 514 (1991).

[7] B. M. Novak, N. Ellsworth, T. I. Wallow, and C. Davies, *Am. Chem. Soc. Div. Polym. Chem. (Polymer Preprtints), 31,* 698 (1990).

[8] F. Suzuki and K. Onozato, *J. Appl. Polym. Sci., 39,* 371 (1990).

[9] I. A. David and G. W. Scherer, *Am. Chem. Soc. Div. Polym. Chem. (Polymer Preprints), 32,* 530 (1991).

[10] G. Phillip and H. Schmidt, *J. Non-Cryst. Solids, 63,* 283 (1984).
[11] H. Schmidt, *Mater. Res. Soc. Symp. Proc., 32,* 327 (1984).
[12] G. L. Wilkes, B. Orler, and H. Huang, *Am. Chem. Soc. Div. Polym. Chem. (Polymer Preprints), 26(2),* 300 (1985).
[13] B. Wang, G. L. Wilkes, J. C. Hedrick, S. C. Liptak, and J. E. McGrath, *Macromolecules (Notes), 24,* 3449 (1991).
[14] B. Tamami, C. Betrabet, and G. L. Wilkes, *Polym. Bull., 30,* 39 (1993).
[15] B. Tamami, C. Betrabet, and G. L. Wilkes, *Polym. Bull., 30,* 393 (1993).
[16] B. Wang and G. L. Wilkes, *Journ. Mac. Sci., Pure & Appl. Chem., A31(2),* 249 (1994).
[17] J. Wen and G. L. Wilkes, *J. Inorg. Organomet. Polym., 5(4),* 343, (1995).
[18] J. Wen, V. J. Vasudevan, and G. L. Wilkes, *J. Sol–Gel Sci. Tech., 5,* 115 (1995).
[19] J. Wen, K. Jordens, and G. Wilkes, in *Better Ceramics Through Chemistry VII: Organic/Inorganic Hybrid Materials (Mater. Res. Soc. Symp. Proc.),* B. K. Coltrain, C. Sanchez, D. W. Schaefer, and G. L. Wilkes, Eds., *435,* 207 (1996).
[20] J. Wen, B. Dhandapani, S. T. Oyama, and G. L. Wilkes, *Chem. Mater., 9(9),* 1968 (1997).
[21] J. Wen and Garth L. Wilkes, *Chem. Mater., 8,* 1667 (1998).
[22] J. Wen and Garth L. Wilkes, in *Polymeric Materials Encyclopedia,* J. C. Salamone, Editor-in-chief, CRC Press, Boca Raton, 1996.
[23] P. Judeinstein and C. Sanchez, *J. Mater. Chem., 6(4),* 511 (1996).
[24] L. Mascia, *Trends in Polym. Sci., 3(2),* 61 (1995).
[25] H. Huang, B. Orler, and G. L. Wilkes, *Polym. Bull., 14,* 557 (1987).
[26] Hao–Hsin Huang, Bruce Orler, and Garth L. Wilkes, *Macromolecules, 20,* 1322 (1987).
[27] Hao–Hsin Huang and Garth L. Wilkes, *Polym. Bull., 18,* 455 (1987).
[28] Raymond H. Glaser and Garth L. Wilkes, *Polym. Bull., 19,* 51 (1988).
[29] Hao–Hsin Huang, Raymond H. Glaser, and Garth L. Wilkes, Chapter 29 in, *Inorganic and Organometallic Polymers (ACS Symp. Ser.), 360,* 354 (1988).
[30] Hao–Hsin Huang, Garth L. Wilkes, and James G. Carlson, *Polymer, 30,* 2001 (1989).
[31] D. E. Rodrigues, A. B. Brennan, C. Betrabet, B. Wang, and G. L. Wilkes, *Chem. Mater., 4(6),* 1438 (1992).

Downloaded At: 12:47 24 January 2011

[32] D. E. Rodrigues and G. L. Wilkes, *J. Inorg. Organomet. Polym., 3(3),* 197 (1993).

[33] N. G. McCrum, B. E. Read, and G. Williams, *Anelastic and Dielectric Effects in Polymeric Solids, reprint of 1967 text,* Dover Publications, Inc., NY, 1991.

[34] L. E. St. Pierre and C. C. Price, *J. Am. Chem. Soc., 78,* 3432 (1956).

[35] R. N. Work, R. D. McCammon, and R. G. Saba, *Bull. Am. Phys. Soc., 8,* 266 (1963).

[36] G. Allen, *Soc. Chem. Ind. Monograph, 17,* 167 (1963).

[37] G. Williams, *Trans. Faraday Soc., 61,* 1564 (1965).

[38] K. Jordens and G. Wilkes, *Journ. Mac. Sci., Pure & Appl. Chem., A37, 3*) (second paper).

[39] V. de Zea Bermudez, L. D. Carlos, M. C. Duarte, M. M. Silva, C. J. R. Silva, M. J. Smith, M. Assunção, and L. Alcácer, *J. Alloys and Compds., 275-277,* 21 (1998).

[40] V. de Zea Bermudez, D. Baril, J.–Y. Sanchez, M. Armand, and C. Poinsignon, in *Optical Materials Technology for Energy Efficient and Solar Energy Conversion XI: Chromogenics for Smart Windows,* A. Hugot–Le Goff, C. G. Granqvist, and C. M. Lampert, Eds., *Proc. SPIE, 1728,* 180 (1992).

[41] V. de Zea Bermudez, L. D. Carlos, and L. Alcácer, *Chem. Mater., 11(3),* 568 (1999).

[42] L. D. Carlos, V. de Zea Bermudez, R. A. Sá Ferreira, L. Marques, and M. Assunção, *Chem. Mater., 11(3),* 581 (1999).

[43] K. Dahmouche, M. Atik, N. C. Mello, T. J. Bonagamba, H. Panepucci, and M. A. Aegerter, *J. Sol–Gel Sci. Tech., **8**,* 711 (1997).

[44] S. J. L. Ribeiro, K. Dahmouche, C. A. Ribeiro, C. V. Santilli, and S. H. Pulcinelli, *J. Sol–Gel Sci. Tech., 13,* 427 (1998).

[45] K. Dahmouche, M. Atik, N. C. Mello, N. C. Mello, T. J. Bonagamba, H. Panepucci, M. A. Aegerter, and P. Judeinstein, *Mater. Res. Soc. Symp. Proc., 435,* 363 (1996).

[46] P. Judeinstein, J. Titman, M. Stamm, and H. Schmidt, *Chem. Mater., 6(2),* 127 (1994).

[47] K. Dahmouche, C. V. Santilli, M. Da Silva, C. A. Ribeiro, S. H. Pulcinelli, and A. F. Craievich, *J. Non-Cryst. Solids, 247,* 108 (1999).

[48] Leroy E. Alexander, *X-ray Diffraction Methods in Polymer Science,* Kreiger Publishing Company, Malabar, FL, 1985.

Downloaded At: 12:47 24 January 2011

[49] L. R. G. Treloar, *The Physics of Rubber Elasticity,* Third Edition, Clarendon Press, Oxford, 1975.

[50] T. M. Miller, L. Zhao, and A. B. Brennan, *J. Appl. Polym. Sci., 68,* 947 (1998).

[51] C. J. Brinker, K. D. Keefer, D. W. Schaefer, R. A. Assink, C. D. Kay, and C. S. Ashley, *J. Non-Cryst. Solids, 63,* 45 (1984).

[52] D. W. Schaefer and K. D. Keefer, in *Better Ceramics Through Chemistry II (Mater. Res. Soc. Symp. Proc.), 73,* 277 (1986).

[53] K. D. Keefer, in *Better Ceramics Through Chemistry (Mater. Res. Soc. Symp. Proc.),* C. J. Brinker, D. E. Clark, and D. R. Ulrich, Eds., *32,* (1984).

[54] Lawrence E. Nielsen, *Mechanical Properties of Polymers and Composites Volume 2,* Marcel Decker, Inc., NY, 1974.

[55] F. R. Schwarzl, H. W. Bree, C. J. Nederveen, G. A. Schwippert, L. C. E. Struik, and C. W. Van der Wal, *Rheol. Acta, 5,* 270 (1966).

[56] R. F. Landel and T. L. Smith, *ARS J., 31,* 599 (1961).

[57] M. Brik, J. Titman, J. P. Bayle, and P. Judeinstein, *J. Polym. Sci.: Part B: Polym. Phys., 34(15),* 2533 (1996).

[58] P. Judeinstein, M. E. Brik, J. P. Bayle, J. Courtieu, and J. Rault, *Mater. Res. Soc. Symp. Proc., 346,* 937 (1994).

[59] F. Surivet, T. M. Lam, J. Pascault, and C. Mai, *Macromolecules, 25(21),* 5742 (1992).

[60] H. Huang, B. Orler, and G. L. Wilkes, *Polym. Bull., 14,* 557 (1987).

[61] H. Huang, B. Orler, and G. L. Wilkes, *Macromolecules, 20,* 1322 (1987).

Received May 5, 1999
Final revision received November 3, 1999

Downloaded At: 12:47 24 January 2011